energies

MDPI

Article

Analysis of Spatiotemporal Predictions and Drivers of Carbon Storage in the Pearl River Delta Urban Agglomeration via the PLUS-InVEST-GeoDetector Model

Jinghang Cai [1], Hui Chi [1,*], Nan Lu [1,*], Jin Bian [1], Hanqing Chen [1], Junkeng Yu [1] and Suqin Yang [2]

[1] Department of Ocean Engineering and Energy, Guangdong Ocean University, Zhanjiang 524088, China; ccc10616@163.com (J.C.); bianjin@gdou.edu.cn (J.B.); hanqing@gdou.edu.cn (H.C.); gqisqa@163.com (J.Y.)
[2] Guangdong Yuehai Water Investment Co., Ltd., Zhanjiang 524088, China; lambsun@126.com
* Correspondence: chihui@gdou.edu.cn (H.C.); lunan@gdou.edu.cn (N.L.)

Abstract: Land use and land cover change (LUCC) significantly influences the dynamics of carbon storage in thin terrestrial ecosystems. Investigating the interplay between land use alterations and carbon sequestration is crucial for refining regional land use configurations, sustaining the regional carbon balance, and augmenting regional carbon storage. Using land use data from the Pearl River Delta Urban Agglomeration (PRDUA) from 2010 to 2020, this study employed PLUS-InVEST models to analyze the spatiotemporal dynamics of land use and carbon storage. Projections for the years 2030, 2040, and 2050 were performed under three distinct developmental scenarios, namely, natural development (ND), city priority development (CPD), and ecological protection development (EPD), to forecast changes in land use and carbon storage. The geographic detector model was leveraged to dissect the determinants of the spatial and temporal variability of carbon storage, offering pertinent recommendations. The results showed that (1) during 2010–2020, the carbon storage in the PRDUA showed a decreasing trend, with a total decrease of 9.52×10^6 Mg, and the spatial distribution of carbon density in the urban agglomeration was imbalanced and showed an overall trend in increasing from the center to the periphery. (2) Clear differences in carbon storage were observed among the three development scenarios of the PRDUA between 2030 and 2050. Only the EPD scenario achieved an increase in carbon storage of 1.10×10^6 Mg, and it was the scenario with the greatest potential for carbon sequestration. (3) Among the drivers of the evolution of spatial land use patterns, population, the normalized difference vegetation index (NDVI), and distance to the railway had the greatest influence on LUCC. (4) The annual average temperature, annual average rainfall, and GDP exerted a significant influence on the spatiotemporal dynamics of carbon storage in the PRDUA, and the interactions between the 15 drivers and changes in carbon storage predominantly manifested as nonlinear and double-factor enhancements. The results provide a theoretical basis for future spatial planning and achieving carbon neutrality in the PRDUA.

Keywords: carbon storage; PLUS-InVEST model; LUCC; geographic detector; multi-scenario simulation

Citation: Cai, J.; Chi, H.; Lu, N.; Bian, J.; Chen, H.; Yu, J.; Yang, S. Analysis of Spatiotemporal Predictions and Drivers of Carbon Storage in the Pearl River Delta Urban Agglomeration via the PLUS-InVEST-GeoDetector Model. *Energies* **2024**, *17*, 5093. https://doi.org/10.3390/en17205093

Academic Editors: Tomasz Kalak and Ryszard Cierpiszewski

Received: 3 September 2024
Revised: 2 October 2024
Accepted: 3 October 2024
Published: 14 October 2024

1. Introduction

Global climate change has received considerable attention in recent years, with greenhouse gas (GHG) emissions, particularly CO_2, being the main drivers [1]. In 2015, the United Nations introduced the sustainable development goals (SDGs), an ambitious set of 17 goals and 167 specific targets, to address a wide array of global challenges, including climate action [2]. Against this backdrop, the Chinese government pledged to actively participate in global climate governance based on its proposal of a double-carbon target at the 2020 UN General Assembly designed to reach peak carbon emissions by 2030 and achieve carbon neutrality by 2060 [1]. Carbon storage denotes the total carbon content of a specific region or ecosystem. Increasing carbon storage in terrestrial ecosystems can effectively reduce atmospheric CO_2 concentrations [3]. Economic development has induced

shifts in land use patterns globally, with the diversity of societal needs and environmental spatial heterogeneity fostering increasingly intricate interactions among ecosystem services that impact carbon sequestration in terrestrial ecosystems and impede sustainable regional development [4–6]. As urban construction land expands, significant areas of forest, cropland, and grassland ecosystems with high carbon sequestration capabilities have been encroached upon, resulting in escalating carbon stock loss within urban ecosystems [7]. Consequently, the rational optimization of land resources is essential for achieving the objectives of land use structure and spatial optimization, enhancing land use efficiency, and combating climate change [8,9]. The simulation of various development scenarios in policy intervention contexts, along with the prediction of future land use and carbon storage changes, allows for the analysis and comparison of differences in simulation results. This provides valuable insights for the study of the ecosystem's carbon balance and is crucial for achieving carbon neutrality goals.

Carbon in terrestrial ecosystems mainly originates from above-and belowground biomass, soil, and dead organic matter, and it is significantly influenced by both natural and human-induced factors [10]. Among these factors, human activities, particularly deforestation and the expansion of built-up areas, have the greatest impact on ecosystem carbon storage through shifts in land use patterns and intensities [11,12]. Currently, many scholars have conducted extensive research on carbon storage estimations, and ecosystem carbon storage estimation methods can be broadly classified into two categories: field sampling and modeling [13,14]. Field sampling estimates and analyzes carbon storage by collecting samples from different land use types, landforms, and soil types. This method is highly accurate but requires significant resources, making it challenging to reflect long-term and large-scale changes in carbon storage [15]. Modeling estimates carbon storage by acquiring regional land use data via remote satellite sensing to calculate carbon density in the study area [16]. Modeling has become the principal method for calculating carbon sinks, owing to its high efficiency and wide applicability.

The most commonly used models for estimating carbon storage include the Carnegie–Ames–Stanford approach (CASA), Carbon and Exchange between Vegetation, Soil, and Atmosphere (CEVSA), and the integrated valuation of ecosystem services and trade-offs (InVEST) [17–19]. InVEST is widely used in multiscale and multi-objective carbon storage assessment studies because of its multi-scenario analysis and time-dynamic features. It is also used when the study area encompasses a range of geographical units, including provinces [20], cities [21], counties [22], agricultural land [23], grasslands [24], forests [25], wetlands [26], and other major ecosystems. The prediction of future spatial distributions of carbon storage necessitates the application of a spatial simulation analysis based on land use types. Many studies have been conducted in this field, and the CA-Markov [27], FLUS [28], and CLUE-S [29] models have been developed to simulate the temporal and spatial dynamic evolution of land use patches. However, these models have demonstrated an insufficient ability to evolve spatiotemporal dynamics. The patch-generating land use simulation (PLUS) model, which is based on a multiclass patch-generation strategy, cannot effectively solve or simulate the complex evolution of multiple classes and scenarios [30].

The integration of the PLUS and InVEST models overcomes their individual limitations, such as the PLUS model's lack of carbon storage calculations and the InVEST model's dependence on multiyear land use data. This approach also enhances the prediction of future land carbon storage dynamics, thereby offering valuable decision-making support for sustainable urban development [31,32]. However, several research gaps remain in the current literature that warrant further investigation. First, current research utilizing the PLUS-InVEST model predominantly focuses on individual provinces or cities, which indicates the need for a more thorough examination of spatiotemporal heterogeneity across urban agglomerations. Second, existing studies have predominantly focused on analyzing and forecasting the patterns of land use and land cover change (LUCC) and carbon storage variations, while the underlying drivers of these changes are poorly understood.

To address the identified research gaps, more thorough examinations of the spatiotemporal heterogeneity within urban agglomerations and further investigations of the underlying drivers of carbon storage are required. Therefore, this study concentrates on the Pearl River Delta Urban Agglomeration (PRDUA), a region in China noted for its economic vitality and land resource shortages. By integrating the PLUS and InVEST models, this research develops three distinct scenarios—natural development (ND), city priority development (CPD), and ecological protection development (EPD)—to simulate and analyze the spatial and temporal dynamics of land use and carbon storage over a 30-year projection period. Furthermore, the geographic detector model and the LEAS module of the PLUS model were utilized to dissect the driving mechanisms behind LUCC and carbon storage variations within the PRDUA, respectively, and their interrelationships were explored in greater depth. The results of this study ensure a systematic and structured approach to investigate the dynamics of LUCC and its implications for carbon storage and will provide a basis for the construction of the future urban and ecological planning pattern of the PRDUA and the realization of China's "Carbon Neutral, Carbon Peak" goal.

The remainder of this paper is structured as illustrated in Figure 1.

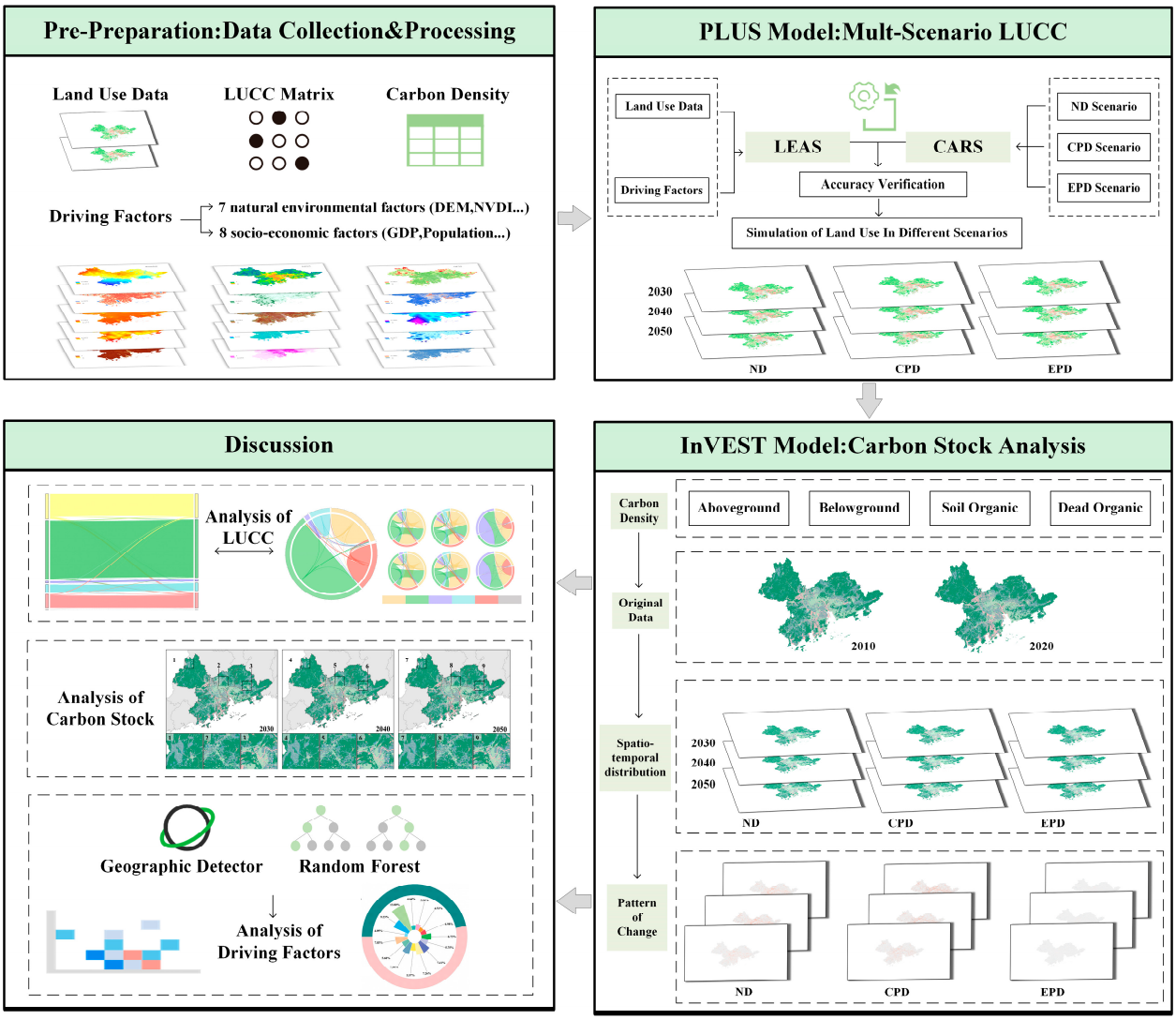

Figure 1. Research framework.

2. Materials and Methods

2.1. Study Area

The PRDUA is situated in the south-central region of Guangdong Province, China, spanning latitudes 20°13′ to 25°31′ N and longitudes 109°39′ E to 117°19′ E. It encompasses a total area of approximately 56,000 km^2 and includes nine cities: Guangzhou, Shenzhen, Foshan, Dongguan, Huizhou, Zhuhai, Zhongshan, Jiangmen, and Zhaoqing (Figure 2). The PRDUA is recognized as one of the most economically vibrant, densely inhabited, and industrially concentrated areas of China. It is characterized by a humid subtropical climate with well-defined seasons, including hot, humid summers and mild, dry winters. The region receives an average annual precipitation of 1600–2300 mm and maintains an average annual temperature range of 21.4–22.4 °C. Its average population is approximately 1,000,000, with some cities having more than 3,000,000 residents.

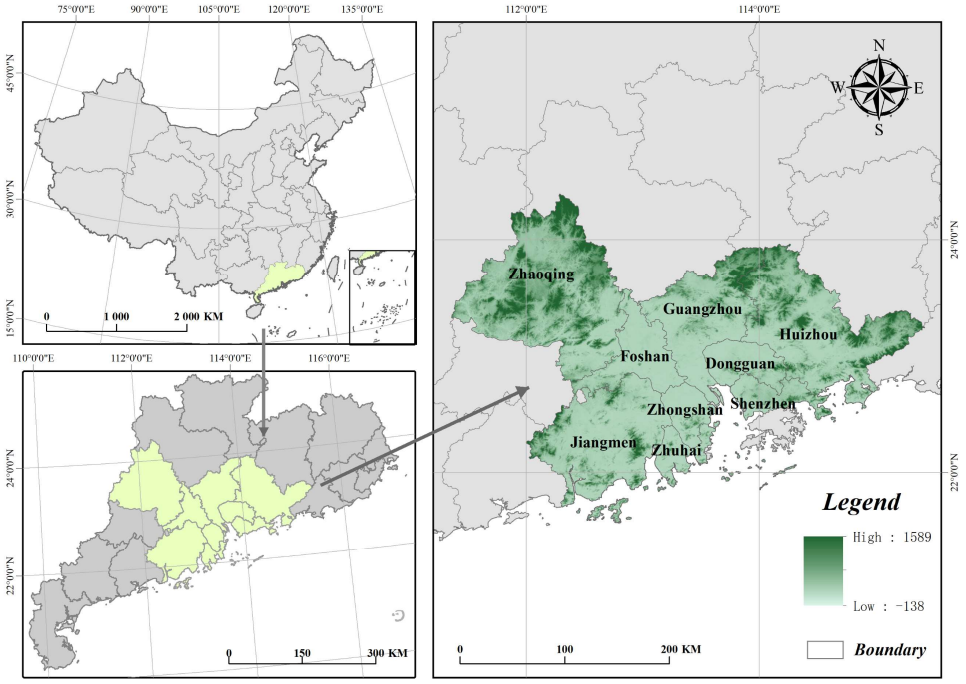

Figure 2. Location of the study area.

As of 2020, the resident population of the PRDUA reached 78.23 million, or approximately 6% of China's total population. Its GDP exceeded RMB 8.9 trillion, or approximately 9% of China's national GDP. With an urbanization rate of 85.9% in 2020, the PRDUA is among the most rapidly urbanized regions in China, exceeding the national average of 26.33% [33]. Guangdong Land Spatial Planning (2021–2035) aims to evolve the PRDUA into a world-class urban agglomeration by integrating and harmonizing diverse specialized planning efforts into a unified land spatial planning framework. This will enhance the land-carrying capacity of the region, which is endowed with rich ecological resources, including the renowned Pearl River Delta water system, wetland reserves, and montane forests. These resources store significant amounts of carbon, which is crucial for maintaining the ecological balance and environmental integrity. However, intensive human development in the region exerts considerable pressure on the regional carbon storage capacity, thereby complicating the carbon cycle mechanisms of urban agglomerations. This complexity presents significant challenges for the systematic assessment and analysis of carbon storage in the PRDUA.

2.2. Methods

2.2.1. PLUS Model

The research framework employs the PLUS model, which integrates the predictive methods of Markov chains. This model is enhanced through optimization and widely used for LUCC analysis and forecasting. It is particularly effective for examining trends in land type, area, and distribution over different periods, making it one of the most commonly employed tools and methodologies for simulating and analyzing land use data. The PLUS model primarily consists of two modules: LEAS and CARS.

Furthermore, the PLUS model incorporates mechanisms such as a stochastic forest-based transportation planning update and a random seed mechanism within planned development areas. These enhancements emphasize the guiding role of transportation planning and planned development zones in the urban development processes. It also addresses a gap in existing research in which only the restrictive effects of planning are accounted for while the driving and guiding influence of planning policies is not considered [34]. By integrating these mechanisms, the PLUS model offers a more nuanced approach to simulating changes in land use and their implications for urban development strategies.

2.2.2. InVEST Model

The InVEST model, grounded in geographic information system (GIS) data and ecological theory, is used to assess and forecast ecosystem services, such as hydrological services, climate regulation, soil conservation, and biodiversity preservation. The InVEST model facilitates the quantitative evaluation and impact analysis of ecosystem services. In this study, we used the predicted land use and revised carbon density categories (aboveground biomass, belowground biomass, soil, and dead organic matter) of the PLUS model to estimate the capacity of the ecosystem for carbon dioxide absorption, storage, and carbon sequestration.

$$C_{total} = \sum A_i \cdot (C_{above} + C_{below} + C_{soil} + C_{dead}) \quad (1)$$

where A_i represents the total area of land use type i (hm^2), C_{above} represents the carbon density of the aboveground biomass (Mg/hm^2), C_{below} represents the carbon density of belowground biomass (Mg/hm^2), C_{soil} represents the carbon density of soil (Mg/hm^2), and C_{dead} represents the carbon density of dead matter (Mg/hm^2).

2.2.3. Scenario Setting

This study utilized land use data from 2010 to 2020 as baseline datasets (hereafter OD2010 and OD2020) to simulate the LUCC of the PRDUA for 2030, 2040, and 2050. Initially, the LEAS module within the PLUS model was employed to obtain the development probabilities and contributions of the driving factors to the expansion of various land use types in the PRDUA from 2010 to 2020. Tables 1 and 2 present the neighborhood weights, which were based on the ratios of land use type expansion to total land expansion and the corresponding transition matrices.

Subsequently, the CARS module was used in conjunction with OD2010, OD2020, and the previously derived development probabilities to establish the three scenarios. The scenario settings, including the reference conditions and transition matrices, are listed in Table 1. The resulting ND, CPD, and EPD scenarios provided LUCC projections in the study area for 2030, 2040, and 2050. By incorporating urban planning policies relevant to the PRDUA, such as the land space planning of Guangdong Province (2021–2035), which stipulates that urban expansion should remain below a factor of 1.3 by 2035, we made appropriate adjustments to the neighborhood factor parameter of construction land under the ND, CPD, and EPD scenarios. Following this approach, we also set the neighborhood factor parameter for other land use types. The transition matrices for the three scenarios are listed in Table 2, where 0 indicates no conversion and 1 indicates that conversion is permitted. The neighborhood weights for each land use type are illustrated in Table 3. The

values ranged from 0 to 1, with higher values denoting greater probabilities of land use conversion.

Table 1. Principles underlying scenario setting.

Scenario	Principles Underlying Scenario Setting
ND	Based on OD2010 and OD2020, the PLUS model summarizes and perpetuates the pattern of change, and scenarios are simulated based on continuous economic development and urbanization to obtain scenarios of natural development without the intervention of special policies (e.g., certain land must be developed under policy conditions).
CPD	In this scenario, urban development is the main focus, with reference to the objective of 'Accelerating the establishment of the Great Bay Area on the railway and driving the synergistic development of the Guangzhou Metropolitan Area, Shenzhen Metropolitan Area, and the Zhuhai-Zhongjiang Region' in the land space planning of Guangdong Province (2021–2035). Moreover, it also considers the land use development plan of the towns in the study area and allows for the conversion of water bodies to construction land. The conversion of water bodies to construction land is allowed, meaning that lake filling or reclamation is allowed for construction. The probability of conversion of other land to construction land is increased by 20%.
EPD	In this scenario, the objective is 'building a low-carbon, ecological, high-efficiency and high-quality urban and rural planning and construction model, and optimizing the spatial pattern of the urban and rural areas' in the integrated urban and rural planning plan for the Pearl River Delta (2009–2020). This scenario includes implementing stringent protection measures for key ecological areas, increasing the area of forests, reducing the rate of reduction in the area of grassland, and limiting the rapid expansion of built-up land. Nature reserves have been added as restricted construction areas; the probability of the conversion of forest and grassland to construction land has been reduced by 30%; the probability of conversion of agricultural land to construction land has been reduced by 50%; and water bodies may not be converted to other land, although other land is allowed to be converted to water bodies.

Table 2. Multiple scenario transfer matrix setting.

Land Use Type	ND						CPD						EPD					
	a	b	c	d	e	f	a	b	c	d	e	f	a	b	c	d	e	f
a	1	1	1	1	1	0	1	1	1	1	1	0	1	1	1	1	1	0
b	1	1	1	1	1	0	1	1	1	1	1	0	0	1	1	0	0	0
c	1	1	1	1	1	0	1	1	1	1	1	0	0	1	1	0	0	0
d	0	0	0	1	0	0	0	0	0	1	1	0	0	0	0	1	0	0
e	0	0	0	0	1	0	0	0	0	0	1	0	0	0	0	0	1	0
f	1	1	1	1	1	1	1	1	1	1	1	1	1	1	1	1	1	1

Note: Letters a–f indicate agricultural land, forest, grassland, water bodies, construction land, and unused land. A value of 1 indicates that the ground class can be converted and 0 indicates that the ground class cannot be converted.

Table 3. Neighborhood factor parameter.

Land Use Type / Scenario	Agriculture Land	Forest	Grassland	Water Body	Construction Land	Unused Land
ND	0.2248	0.1636	0.0498	0.1236	0.4379	0.0002
CPD	0.1124	0.0818	0.0249	0.0618	0.8758	0.0001
EPD	0.2248	0.3273	0.0997	0.1236	0.4379	0.0002

2.2.4. LUCC Accuracy Calibration and Verification

To ensure the reliability of the predictive scenario outputs of the model, the kappa coefficient was employed to validate the accuracy of the LUCC data from OD2010 and OD2020 by comparing the simulated results with actual observations. This process verified the reliability of the LUCC data for 2010 and 2020. The kappa coefficient is based on the following principle:

$$kappa = \frac{p_o - p_e}{1 - p_e} \tag{2}$$

where p_e represents the sum of correctly classified samples for each category divided by the total number of samples, which is the overall classification accuracy. Let the true number of samples for each category be $a_1, a_2, \ldots, a_c$ and the predicted number of samples for each

category be b_1, b_2, …, bc. Then, given the total number of samples n, the following equation was obtained:

$$p_e = \frac{a_1 \times b_1 + a_2 \times b_2 + \ldots + a_C \times b_C}{n \times n} \quad (3)$$

The kappa coefficients ranged from 0 to 1, with intervals of 0.2 defining the grades of agreement. Higher values indicated greater predictive concordance [35]. The kappa coefficient is categorized into five levels: slight (0.00–0.20), fair (0.21–0.40), moderate (0.41–0.60), substantial (0.61–0.80), and almost perfect (0.81–1.00). In this study, the kappa prediction result for land use forecasting was 0.875335 (approximately 0.88), which falls into the almost perfect category. This suggests a high degree of consistency between the initial data and the actual LUCC conditions, thereby ensuring data reliability.

2.2.5. Geographical Detector Model

The geographical detector model is an effective tool for identifying interactions between drivers and dependent variables and for measuring the driving force of spatial differentiation mechanisms. The data discretization method used in this study is the geodetector "GD" R package (4.4.1) and is used to reveal the explanatory power of certain factors on carbon stocks. The q-value, which represents a key indicator of the explanatory power of factor X on the spatial variability of attribute Y, ranges from 0 to 1, with a higher value indicating stronger explanatory power of the factor on carbon stocks from 0 to 1 and a stronger explanatory power of the factors on carbon storage. The formula is as follows:

$$q = 1 - \frac{\Sigma_{h=1}^{L} N_h \sigma_h^2}{N\sigma^2} = 1 - \frac{SSW}{SST} \quad (4)$$

where h = 1, …, L denotes the classification of variable Y or factor X; N_h and N denote the number of layers at level h and total number of units, respectively; σ_h^2 represents the variance within the Y values for class h; and σ^2 denotes the overall variance of the Y values. SSW indicates the sum of variances within each stratum and SST represents the total variance across all classes.

2.3. Data Sources

2.3.1. Remote Sensing Dataset of LUCC

LUCC predictions in this study were based on OD2010 and OD2020, both sourced from the unified classification system of the Chinese Academy of Sciences from the Resource and Environmental Science and Data Center (RESDC, https://www.resdc.cn, accessed on 5 April 2023). The datasets were reclassified into primary land cover types according to the Chinese land use classification system (GB/T21010-2007) using ArcGIS. This reclassification encompasses six categories: agricultural land, forest, grassland, water bodies, construction areas, and unused land. Prior to the subsequent analysis, the data were transformed into primary classifications with a spatial resolution of 30 m.

2.3.2. Driving Factor Data

To enhance the alignment between the predicted outcomes and real-world scenarios in the application of the PLUS model under multiple scenarios, 15 driving factors were incorporated, and they included seven natural environmental and eight socioeconomic factors. In this study, the selected driving factors were categorized into two main groups for analysis: socioeconomic and natural environmental. Socioeconomic factors such as population growth and GDP drive increased demand for residential and commercial land use, which, in turn, influences urban planning and shifts in land use types. These changes significantly impact land use patterns, ultimately affecting carbon storage. Moreover, interplay is observed between these factors. For instance, population size influences GDP growth and changes in socioeconomic factors lead to alterations in ecosystems, which in turn result in corresponding shifts in natural environmental factors. The classification of the data types and their sources is detailed in Table 4, with specific illustrations being

provided in Figure 3. After resampling, a grid resolution of 30 m × 30 m was achieved using ArcMap.

Table 4. Details of the driving factor data.

Category	Data	Data Resource	Original Resolution (m)
Socioeconomic Factors	Population	Open Spatial Demographic Data and Research (https://www.worldpop.org/, accessed on 5 April 2023)	100
	GDP	Global Change Research Data Publishing and Repository (http://www.geodoi.ac.cn, accessed on 6 April 2023)	1000
	Distance to railway Distance to expressway Distance to trunk road Distance to the secondary trunk road Distance to the city center Distance to river	OpenStreetMap (https://www.openstreetmap.org/, accessed on 10 April 2023)	90
Natural Environmental Factors	Soil	National Qinghai–Tibet Plateau Scientific Data Center (http://data.tpdc.ac.cn/, accessed on 13 April 2023)	1000
	NDVI	Earthdata Search (https://search.earthdata.nasa.gov/search, accessed on 20 April 2023)	250
	Annual average temperature Annual average rainfall	WorldClim (https://worldclim.org/data/index.html, accessed on 11 April 2023)	490
	DEM Slope Aspect of slope	Geospatial Data Cloud (http://www.gscloud.cn, accessed on 6 April 2023)	30

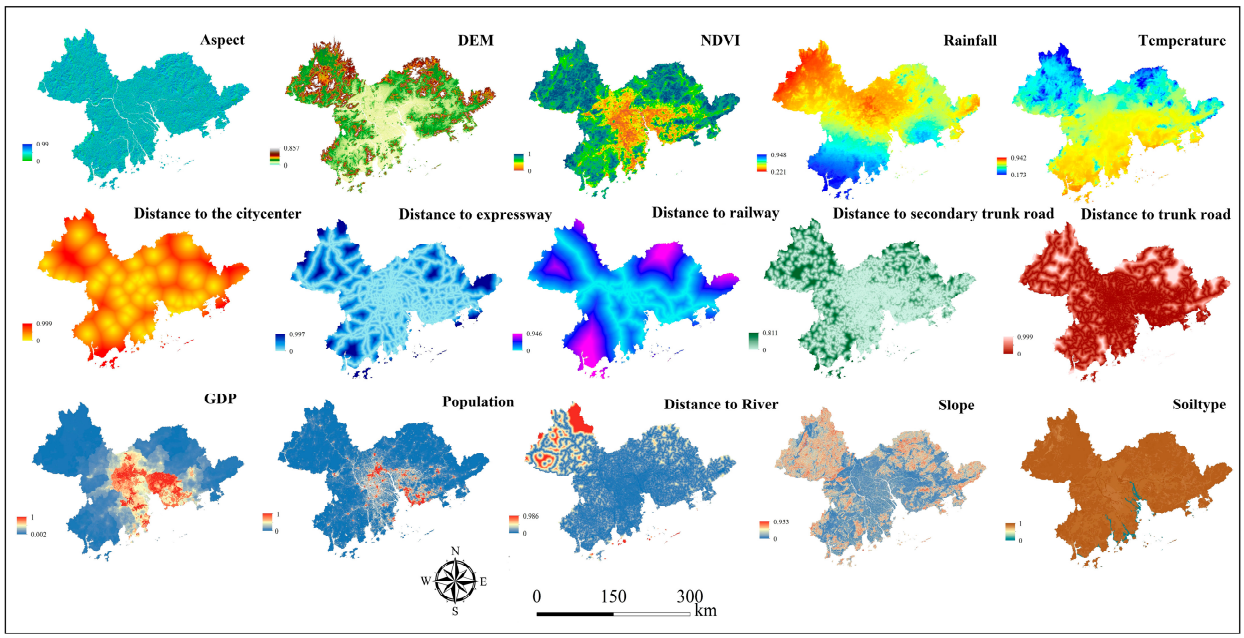

Figure 3. Drivers of LUCC in the PRDUA.

2.3.3. Carbon Density Data

Carbon density refers to carbon storage per unit area and encompasses four carbon pools: aboveground carbon density, belowground carbon density, soil organic carbon density, and dead organic matter carbon density [36]. The carbon density coefficients used in this study were obtained from the National Ecology Science Data Center (http://www.cnern.org.cn/) and Wang et al. [37]. To assess regional carbon density thresholds from a land use type macro perspective, we also considered geographical factors, such as climate, temperature, hydrology, and ecology. The values listed in Table 5 were obtained by applying the correction formula proposed by Zhang et al. [38]. The carbon

density obtained after calibration could be uniformly applied to all land use types within the study area.

$$C_{SP} = 3.3968 \times MAP + 3996.1\left(R^2 = 0.11\right) \quad (5)$$

$$C_{BP} = 6.798 \times e^{0.0054 \times MAP}\left(R^2 = 0.70\right) \quad (6)$$

$$C_{BT} = 28 \times MAT + 398\left(R^2 = 0.477, p < 0.01\right) \quad (7)$$

$$K_{BP} = \frac{C'_{BP}}{C_{BP}} \quad (8)$$

$$K_{BT} = \frac{C'_{BT}}{C_{BT}} \quad (9)$$

$$K_B = K_{BP} \times K_{BT} = \frac{C'_{BP}}{C_{BP}} \times \frac{C'_{BT}}{C_{BT}} \quad (10)$$

$$K_S = \frac{C'_{SP}}{C_{SP}} \quad (11)$$

Table 5. Carbon density of each land use type in the area (t/hm^2).

Land Use Type	Aboveground	Belowground	Soil Organic	Dead Organic Matter	Total
Agriculture land	31.32	2.16	86.17	1.17	120.82
Forest	49.25	17.92	171.7	7.61	246.48
Grassland	2.38	11.23	68.08	2.22	83.91
Water body	0.05	0	0	0	0.05
Construction land	0.26	2.01	61.78	0	64.05
Unused land	0.43	0	62.87	0	63.3

3. Results

3.1. Spatiotemporal Analysis of Carbon Storage in the PRDUA from 2010 to 2020

3.1.1. Analysis of LUCC in the PRDUA from 2010 to 2020

Using ArcGIS software (10.8.1), this study analyzed the land use transfer characteristics of the PRDUA region from 2010 to 2020. The results are presented in Table 6. From the perspective of the land use dynamic degree (hereinafter referred to as K), the PRDUA region primarily exhibited increases in construction land and grassland but showed significant declines in other land types, such as agricultural land, forest, water bodies, and unused land.

Table 6. Land use area and its changes in OD2010 and OD2020.

Land Use Type	2010	2020	2010–2020	K *
Agriculture land	12,596.73	12,049.51	−547.22	−0.43%
Forest	29,428.98	29,043.33	−385.65	−0.13%
Grassland	949.3434	1031.603	82.26	0.87%
Water body	4046.033	3975.3774	−70.66	−0.18%
Construction land	7137.203	8089.844	952.64	1.33%
Unused land	38.1159	6.7446	−31.37	−8.23%

Note: * K is the annual rate of change in land use type during the study period.

Land use changes impacted 1034.90 km^2 of the PRDUA region. In 2020, forests were the most extensively distributed land cover type, covering an area of 29,043.33 km^2, representing approximately 53.59% of the total area. From 2010 to 2020, forested areas decreased by 385.65 km^2, accounting for approximately 37% of the total area reduction in the research region. Agricultural land occupied an area of 12,596.73 km^2 in 2020, representing approximately 22.23% of the total area. Agricultural land experienced a marked decline from 2010 to 2020, with a total reduction of 547.22 km^2, accounting for approximately

52.88% of the overall decrease, with a K value of 0.43%. Agriculture land was the land type with the largest proportional reduction in land uses. Construction land was predominantly concentrated in the central region of the PRDUA at lower elevations. Construction land expanded by 952.64 km^2, representing approximately 92.05% of the total increase, with a K value of 1.33%, indicating significant expansion. The grassland area increased by 82.26 km^2, with a K value of 0.87%.

3.1.2. Spatial and Temporal Evolution Characteristics of Land Use

In the PRDUA, an area of approximately 1034.90 km^2 was affected by the land use transition between 2010 and 2020, approximately 1.91% of the total study area. Construction land, agricultural land, and forest land were the primary types of transformation during the study period. The net increase in construction land was 952.64 km^2, whereas the net decreases in agricultural land and forest land were 547.22 km^2 and 385.65 km^2, respectively.

Agricultural land accounted for the largest area of transferred land, with the majority being converted to construction (861.83 km^2) and forest (312.74 km^2) land, amounting to a total of 1174.56 km^2, approximately 82.59% of the total agricultural land conversion. The largest proportion of forest land was converted to urban (473.29 km^2) and agricultural (336.84 km^2) land, amounting to 810.13 km^2, representing approximately 79.22% of the total forest land conversion.

The distribution of land use types in the study area as a whole presented a circular outward trend. Construction land was mainly distributed in the south-central part of the study area and concentrated in Guangzhou, Shenzhen, Dongguan, Foshan, and Zhuhai, and it showed a tendency to expand toward the respective city boundaries. Agricultural land was distributed on the periphery of construction land and showed a trend towards significant reduction with the conversion of construction land. Forests were distributed over the widest area and mainly located in the northeast, northwest, and southwest of the study area, being clustered mainly in Zhaoqing, Huizhou, and Jiangmen. Grassland, water bodies, and unused land occupied smaller areas, and the overall change was slight and more balanced.

The results of the analysis showed that unused land and forests were significantly affected by this expansion, with construction land being the fastest-growing type. The transition of land use areas occurred primarily in construction, forest, and agricultural land, whereas changes in grassland, water bodies, and unused land remained relatively stable and balanced (Figure 4).

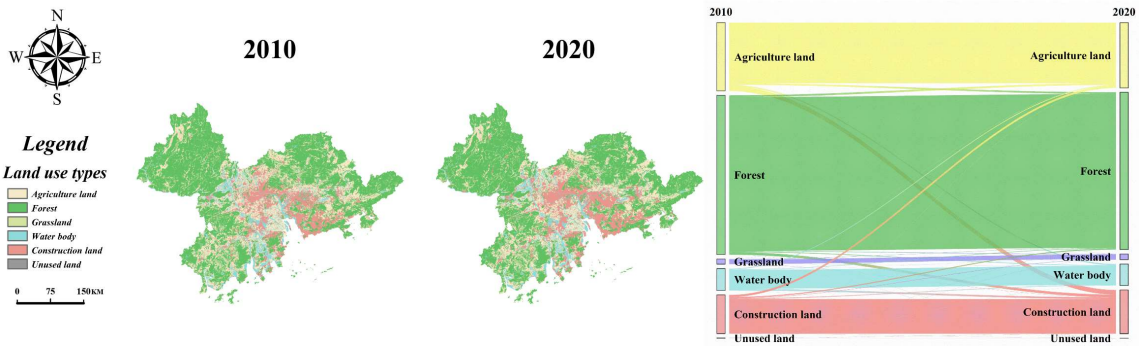

Figure 4. Distribution of land use types and a Sankey diagram of mutual conversion.

3.1.3. Patterns in Carbon Storage Changes in the PRDUA from 2010 to 2020

Using the carbon storage calculation module of the InVEST model, we computed the carbon reserves for the PRDUA region in 2010 and 2020 to determine the spatiotemporal changes in carbon storage. The results indicated that the carbon reserves in 2010 and 2020 were 931.50 $\times$ 10^6 Mg and 921.98 $\times$ 10^6 Mg, respectively, showing an overall declining trend with a carbon loss of 9.52 $\times$ 10^6 Mg, a decrease of 1.02%. The primary cause of this decrease was rapid urbanization being pursued as a development goal and a key task during this period, as outlined in the Pearl River Delta Region Reform and Development Plan

(2008–2020), with an urbanization rate exceeding 85% by the end of 2020. Consequently, the region experienced a significant industrial development, which accelerated the expansion of construction land through a reduction in forest, grassland, and agricultural land, with a subsequent decline in carbon storage (Figure 5).

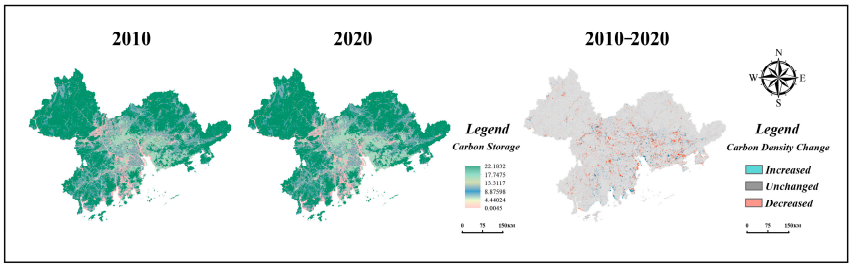

Figure 5. Distribution of carbon storage and areas where carbon storage changed.

In terms of spatial distribution, cities in the PRDUA exhibited considerable heterogeneity in their carbon reserves in 2020. High-carbon reserve areas were predominantly located in the northeastern, northwestern, and southwestern parts of the study area, mainly in Huizhou, Zhaoqing, and Jiangmen. The areas on the periphery of the study region have high vegetation coverage and good ecological benefits. The land use types were primarily agricultural land and forests with lower urbanization rates where the carbon density reached a maximum of 22.1800 Mg/hm^2. Low carbon reserve areas were mainly concentrated in the central region of the study area, particularly in Guangzhou, Shenzhen, Foshan, and Dongguan. These cities have higher urbanization levels, intense human disturbance, and a higher per capita GDP, with land being primarily used for urban development. The carbon density in these areas was as low as 0.0045 Mg/hm^2.

3.2. Analysis of LUCC in the PRDUA under Multi-Scenario Simulations from 2020 to 2050

Land use change in the PRDUA was simulated for three scenarios (ND, CPD, and EPD) using 2030, 2040, and 2050 as temporal milestones with 10-year intervals, as illustrated in Figure 6 and Table 7. The transfers between land types under the three simulated scenarios are shown in Figure 7.

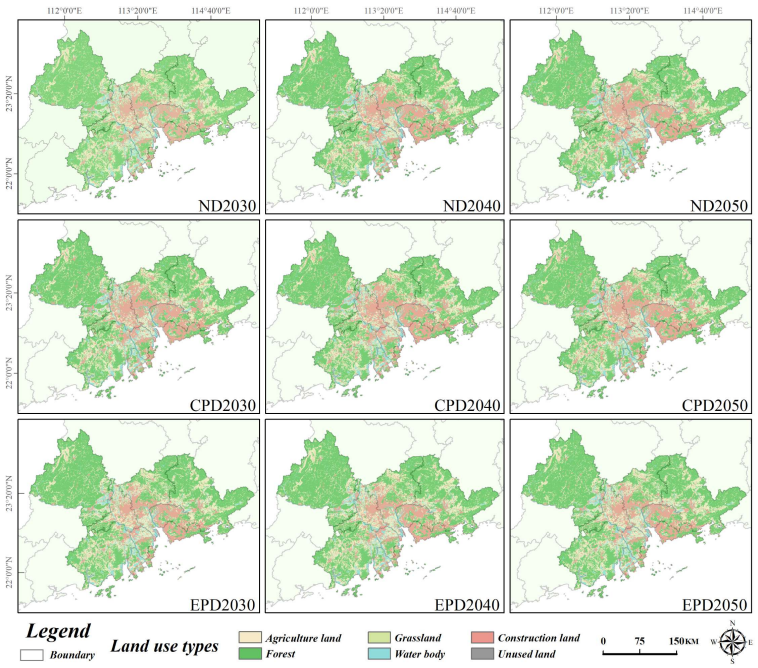

Figure 6. Distribution of land use types under the multi-scenario simulations in 2030–2050.

Table 7. Area of OD2020 and future land use under the three simulated scenarios and the change area of each land use type under the three scenarios (10-year intervals) (km^2).

Period		Agriculture Land	Forest	Grassland	Water Body	Construction Land	Unused Land
OD	2020	12,049.51	29,043.33	1031.60	3975.38	8089.84	6.74
ND	2030	11,609.30	28,684.91	960.25	4060.40	8876.30	5.24
	2040	11,256.08	28,351.34	922.73	4122.51	9539.11	4.63
	2050	10,974.11	28,040.73	914.01	4162.28	10,101.01	4.26
	2020–2030	−440.21	358.42	−71.35	85.03	786.46	−1.5
	2030–2040	−353.21	−333.57	−37.52	62.11	662.81	−0.61
	2040–2050	−281.97	−310.6	−8.72	39.77	561.89	−0.37
CPD	2030	11,448.75	28,587.06	924.04	4028.73	9204.03	3.78
	2040	10,975.14	28,163.65	857.09	4067.05	10,130.58	2.88
	2050	10,603.87	27,770.5	827.74	4085.79	10,906.05	2.46
	2020–2030	−600.75	−456.27	−107.57	53.36	1114.19	−2.96
	2030–2040	−473.61	−423.41	−66.94	38.32	926.55	−0.9
	2040–2050	−371.27	−393.15	−29.36	18.74	775.47	−0.42
EPD	2030	12,003.69	29,127.25	948.55	3975.60	8135.76	5.56
	2040	11,971.08	29,157.46	918.54	3975.60	8168.20	5.52
	2050	11,949.24	29,169.13	906.98	3975.63	8189.88	5.54
	2020–2030	−45.81	83.92	−83.05	0.22	45.92	−1.19
	2030–2040	−32.61	30.2148	−30.01	0.01	32.44	−0.04
	2040–2050	−21.84	11.67	−11.56	0.03	21.68	0.01

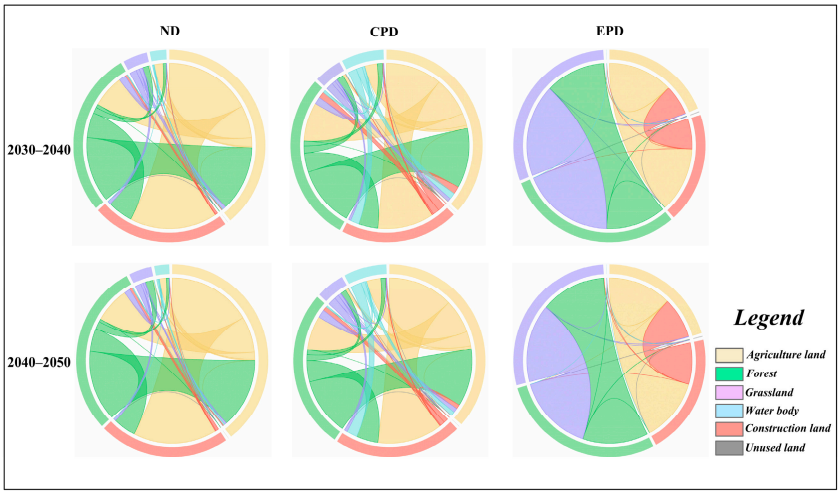

Figure 7. Interconversion of land use types under the multi-scenario simulation in 2030–2050.

3.2.1. ND Scenario

Under the ND scenario, the overall trends in land area changes across the three time periods were consistent, with significant reductions in agricultural and forested areas and a substantial increase in construction land. Specifically, from 2020 to 2030, agricultural land decreased by 440.21 km^2 (50.51% of the total reduction), forest land decreased by 358.42 km^2 (41.13% of the total reduction), and construction land expanded by 786.46 km^2 (92.05% of the total increase). From 2030 to 2040, agricultural land decreased by 353.21 km^2 (48.72% of the total reduction), forest land decreased by 333.57 km^2 (46.02% of the total reduction), and construction land increased by 662.81 km^2 (91.43% of the total increase). From 2040 to 2050, agricultural land decreased by 281.97 km^2 (46.87% of the total reduction), forest land decreased by 310.60 km^2 (51.62% of the total reduction), and construction land expanded by 561.8934 km^2 (93.39% of the total increase). Overall, the proportion

of agricultural land decreased over time while the proportion of forest land increased incrementally. The expansion of construction land was primarily concentrated in the central region, spread outward, and showed an upward trend.

3.2.2. CPD Scenario

Under the CPD scenario, the patterns of change in agricultural, forest, and construction land were generally consistent with those under the ND scenario. From 2020 to 2030, agriculture land decreased by 600.75 km^2 (51.45% of the total reduction), forest land decreased by 456.27 km^2 (39.08% of the total reduction), and construction land expanded by 1114.1892 km^2 (95.43% of the total increase), which represented the largest expansion in construction land among all the scenarios. From 2030 to 2040, agriculture land decreased by 473.61 km^2 (49.09% of the total reduction), forest land decreased by 423.41 km^2 (43.88% of the total reduction), and construction land increased by 926.55 km^2 (96.03% of the total increase). From 2040 to 2050, agricultural land decreased by 371.27 km^2 (46.75% of the total reduction), forest land decreased by 393.15 km^2 (49.50% of the total reduction), and construction land expanded by 775.47 km^2 (97.64% of the total increase). Overall, compared to the ND scenario, the reduction in agricultural and forest land was more pronounced and the growth rate of construction land increased significantly, with its contribution to the total reaching 97.64% by 2050.

3.2.3. EPD Scenario

Under the EPD scenario, agricultural land and grassland decreased while forests and construction land generally increased. From 2020 to 2030, agricultural land decreased by 45.81 km^2 (35.23% of the total reduction) and grassland decreased by 83.05 km^2 (63.86% of the total reduction). However, forest land increased by 83.92 km^2 (64.53% of the total increase) and construction land increased by 45.92 km^2 (35.31% of the total increase). From 2030 to 2040, agricultural land decreased by 32.61 km^2 (52.05% of the total reduction) and grassland decreased by 30.01 km^2 (47.90% of the total reduction). However, forest land increased by 30.21 km^2 (48.22% of the total increase) and construction land increased by 32.44 km^2 (51.77% of the total increase). From 2040 to 2050, agricultural land decreased by 21.84 km^2 (65.40% of the total reduction) and grassland by 11.56 km^2 (34.61% of the total reduction). However, forest land increased by 11.67 km^2 (34.95% of the total increase) and construction land by 21.68 km^2 (64.94% of the total increase). Compared with the previous two scenarios, the EPD scenario led to continued decreases in agricultural land and grassland continued to decrease, with the largest reduction occurring from 2020 to 2030 at 45.81 km^2 and 83.05 km^2, respectively. However, forest land showed a sharp increase, which is in contrast to the decreases observed in the previous two scenarios. Construction land also continued to increase, although its growth rate was significantly constrained by the sharp increase in forest land.

3.3. Spatiotemporal Change of Carbon Storage in the PRDUA under Multi-Scenario Simulation

3.3.1. Temporal Change

The PLUS and InVEST models were used to calculate the carbon storage outcomes for 2030, 2040, and 2050 under three distinct scenarios, as detailed in Table 8. Generally, carbon storage in the PRDUA exhibited a declining trend in both the ND and CPD scenarios, which implies that, if the prevailing development patterns are left unchecked or a development strategy that emphasizes urban primacy is pursued, the PRDUA would be confronted by the daunting prospect of significant "carbon loss". Accordingly, realizing the goal of sustainable development and the target of "carbon neutrality" would be exceptionally difficult. Conversely, in the EPD scenario, the decline in agricultural and grassland areas was more moderate and complemented by a consistent increase in forest land, which collectively contributed to a stable carbon sequestration effect, thereby maintaining carbon storage stability within the urban agglomeration.

Table 8. Carbon storage ($\times 10^6$ Mg) and ratio (%) for land use types under three scenarios in 2030, 2040, and 2050.

Period		Agriculture Land (Rate%)	Forest (Rate%)	Grassland (Rate%)	Water Body (Rate%)	Construction Land (Rate%)	Unused Land (Rate%)	Total
OD	2010	152.19 (16.34%)	725.37 (77.87%)	7.97 (0.86%)	0.0202 (0.0022%)	45.71 (4.91%)	0.2413 (0.0259%)	931.50
	2020	145.58 (15.79%)	715.86 (77.64%)	8.66 (0.94%)	0.0199 (0.0022%)	51.82 (5.62%)	0.0427 (0.0046%)	921.98
ND	2030	140.26 (15.38%)	707.03 (77.50%)	8.06 (0.88%)	0.0203 (0.0022%)	56.85 (6.23%)	0.0332 (0.0036%)	912.25
	2040	136.00 (15.05%)	698.80 (77.33%)	7.74 (0.86%)	0.0206 (0.0023%)	61.10 (6.76%)	0.0293 (0.0032%)	903.69
	2050	132.59 (14.80%)	691.15 (77.12%)	7.67 (0.86%)	0.0208 (0.0023%)	64.70 (7.22%)	0.0270 (0.0030%)	896.15
CPD	2030	138.32 (15.21%)	704.61 (77.46%)	7.75 (0.85%)	0.0201 (0.0022%)	58.95 (6.48%)	0.0240 (0.0026%)	909.69
	2040	132.60 (14.75%)	694.18 (77.23%)	7.19 (0.80%)	0.0203 (0.0023%)	64.89 (7.22%)	0.0183 (0.0020%)	898.90
	2050	128.12 (14.40%)	684.49 (76.96%)	6.95 (0.78%)	0.0204 (0.0023%)	69.85 (7.85%)	0.0156 (0.0018%)	889.44
EPD	2030	145.03 (15.71%)	717.93 (77.78%)	7.96 (0.86%)	0.0199 (0.0022%)	52.11 (5.65%)	0.0352 (0.0038%)	923.08
	2040	144.63 (15.66%)	718.67 (77.83%)	7.71 (0.83%)	0.0199 (0.0022%)	52.32 (5.67%)	0.0350 (0.0038%)	923.39
	2050	144.37 (15.63%)	718.96 (77.86%)	7.61 (0.82%)	0.0199 (0.0022%)	52.46 (5.68%)	0.0350 (0.0038%)	923.45

From 2020 to 2050, the PRDUA experienced a greater reduction in carbon storage in the CPD scenario than in the ND scenario. In the ND scenario, the total carbon storage decreased by 25.82 $\times$ 10^6 Mg, with phased reductions of 9.72 $\times$ 10^6 Mg, 8.56 $\times$ 10^6 Mg, and 7.54 $\times$ 10^6 Mg, for 2020–2030, 2030–2040, and 2040–2050, respectively. Under the CPD scenario, the total carbon storage decreased by 32.54 $\times$ 10^6 Mg, with phased reductions of 12.29 $\times$ 10^6 Mg, 10.79 $\times$ 10^6 Mg, and 9.46 $\times$ 10^6 Mg for 2020–2030, 2030–2040, and 2040–2050, respectively. Both scenarios were characterized by substantial decreases in agricultural land, forest land, and grassland; conversely, the area of land used for construction significantly increased, whereas water bodies and unutilized land remained relatively stable. The more pronounced intensity of land transformation under the CPD scenario contributed to the larger magnitude of carbon storage reduction.

Over time, the rate of decrease in total carbon storage in the PRDUA decreased in both scenarios, which may be attributed to inherent limitations on land use conversion. However, this was not sufficient to counterbalance the carbon loss resulting from the expansion of construction land. In the CPD scenario, the PRDUA witnessed a slight net increase in total carbon storage, amounting to a cumulative gain of 1.48 $\times$ 10^6 Mg, with respective increments of 1.10 $\times$ 10^6 Mg, 0.31 $\times$ 10^6 Mg, and 0.07 $\times$ 10^6 Mg across the three stages. A peak of 923.45 $\times$ 10^6 Mg was reached by 2050, which was the highest in its historical evolution. In this scenario, various land types remain stable, leading to relatively minimal changes in carbon storage. However, the rapid contraction in the expansion of built-up areas to protect the ecological environment suggests that prioritizing the environment may impact the pace of economic development, potentially resulting in an imbalance between human development and ecological conservation.

3.3.2. Spatial Evolution

The carbon storage distribution in the PRDUA under different development scenarios from 2030 to 2050 is illustrated in Figure 8. The spatial patterns in the low-carbon storage areas were generally consistent with those observed from 2010 to 2020, with low values being predominantly concentrated in the central and southern parts of the region and high values being scattered in the northeast, northwest, and southwest regions. Nevertheless, under

varying developmental constraints, the carbon storage patterns under the three scenarios exhibited distinct differences. The pursuit of cooperative development among cities within the urban agglomeration and the continuous expansion of built-up areas toward intercity borders led to a significant expansion of low-carbon storage areas in the CPD scenario, with the ND scenario exhibiting a slightly smaller range, primarily along the boundaries of economically prosperous cities. In contrast, restrictions on urban expansion and initiatives to promote the "Grain for Green Project" and reforestation contributed to the EPD scenario's high carbon storage values.

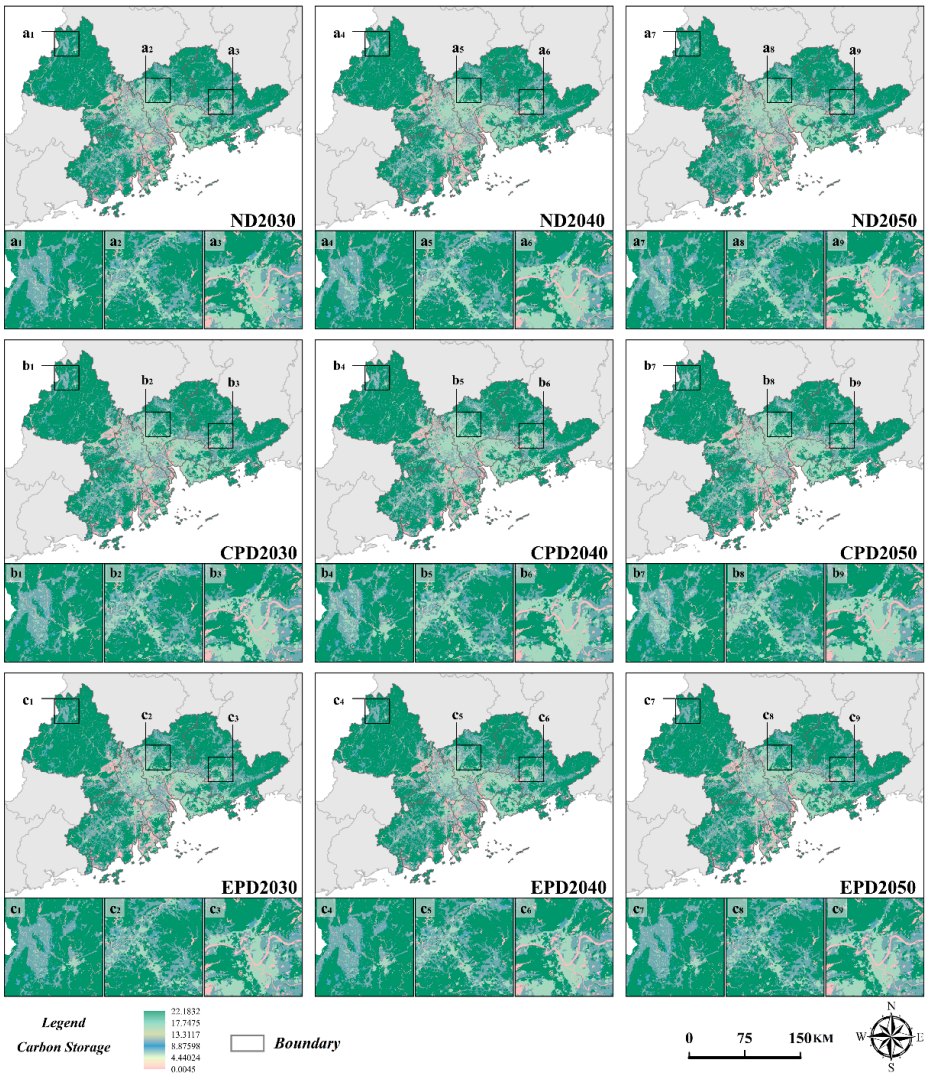

Figure 8. Map of high and low carbon storage distribution areas and their refinement under a multi-scenario simulation (a1, a4, a7, b1, b4, b7, c1, c4, c7 represent the same area; a2, a5, a8, b2, b5, b8, c2, c5, c8 represent the same area; a3, a6, a9, b3, b6, b9, c3, c6, c9 represent the same area).

Next, we analyzed the spatial and temporal variations in carbon storage to delineate the spatiotemporal dynamics of the carbon storage changes in the PRDUA over time. Changes were categorized into three distinct classes: "increase", "decrease", and "no change". The results are presented in Figure 9. Under the ND scenario, the carbon storage distribution within the PRDUA demonstrated a pattern characterized by small-scale scattered increases at the periphery and widespread scattered decreases in the central region. Over 30 years, the focus of carbon loss was on the central part of the study area, particularly in Guangzhou and Foshan, mainly as a result of the swift expansion of built-up areas, converting high-carbon-density agricultural land and forest land into low-carbon-density construction land. Regions with notable increases in carbon storage

were predominantly small and isolated, yet their overall impact was minimal. Interestingly, localized carbon accumulation was also observed in the central zones that experienced significant carbon loss. In the CPD scenario, the extent of the scattered decreases in the central regions expanded outward and became relatively concentrated compared with the ND scenario. Urban greening initiatives have contributed to an increase in carbon storage. Under the EPD scenario, stringent forest protection and enhanced reforestation efforts led to substantial carbon sequestration. Simultaneously, measures were implemented to safeguard agricultural land and grasslands, thereby reducing the transition rate. In this scenario, the areas with decreased carbon storage were significantly reduced, whereas those with increased carbon storage expanded. As economic development progressed, cities continued to grow, and the ecological benefits of this scenario became more pronounced in areas where carbon neutrality had been achieved.

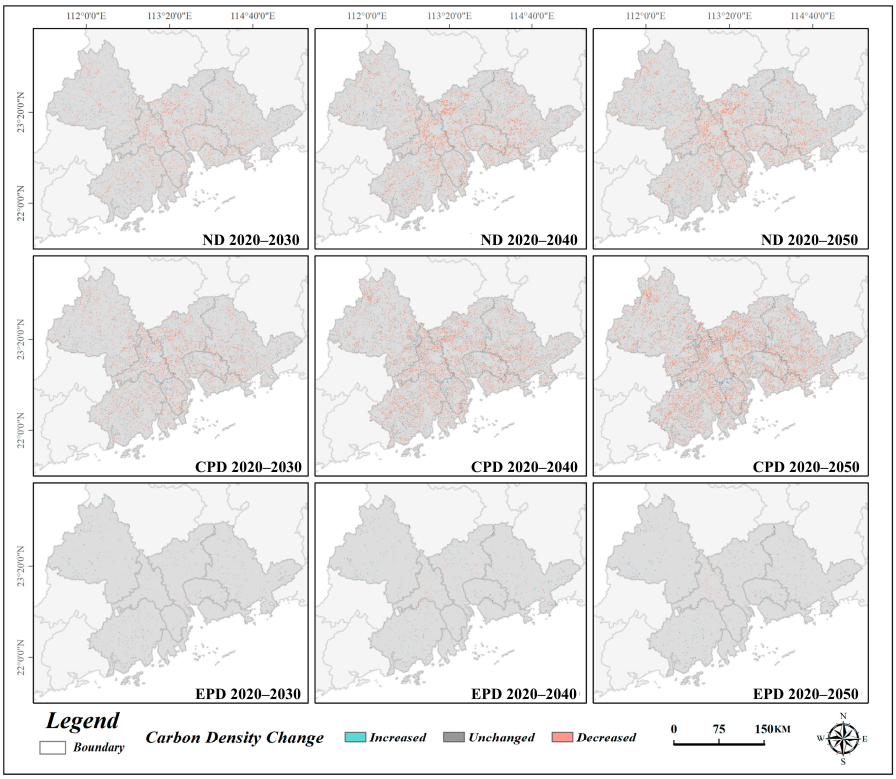

Figure 9. Distribution area of carbon storage changes under multi-scenario simulation.

3.4. Driving Mechanisms of the Spatiotemporal Variability in LUCC and Carbon Storage

3.4.1. Driving Mechanisms of the LUCC in LEAS Module of the PLUS Model

The driving mechanisms of the LUCC in LEAS module of the PLUS model calculated the contribution value of 15 drivers of changes to land use types, including seven natural environmental factors and eight socioeconomic factors. The results are presented in Figure 10.

The main factors affecting carbon storage were population, the normalized difference vegetation index (NDVI), the digital elevation model (DEM), and the distance to the railway. The impact of GDP on the six types of land use was relatively balanced, exceeding a 6.00% contribution for each type. For agricultural, forest, and construction land, the most significant driving factor was NDVI, with contributions reaching 10.99%, 15.02%, and 15.27%, respectively. The three primary drivers affecting grassland were population, distance to the city center, and DEM, with respective contributions of 18.10%, 15.37%, and 14.69%; the drivers were dominated by natural environmental factors and socioeconomic factors. For water bodies, the two most substantial driving factors were DEM and distance to the river, with contributions of 18.13% and 11.84%, respectively, and the drivers were

dominated by socioeconomic factors. The three most influential factors on unused land were distance to the railway, NDVI, and GDP, with contributions of 21.82%, 18.91%, and 13.64%, respectively.

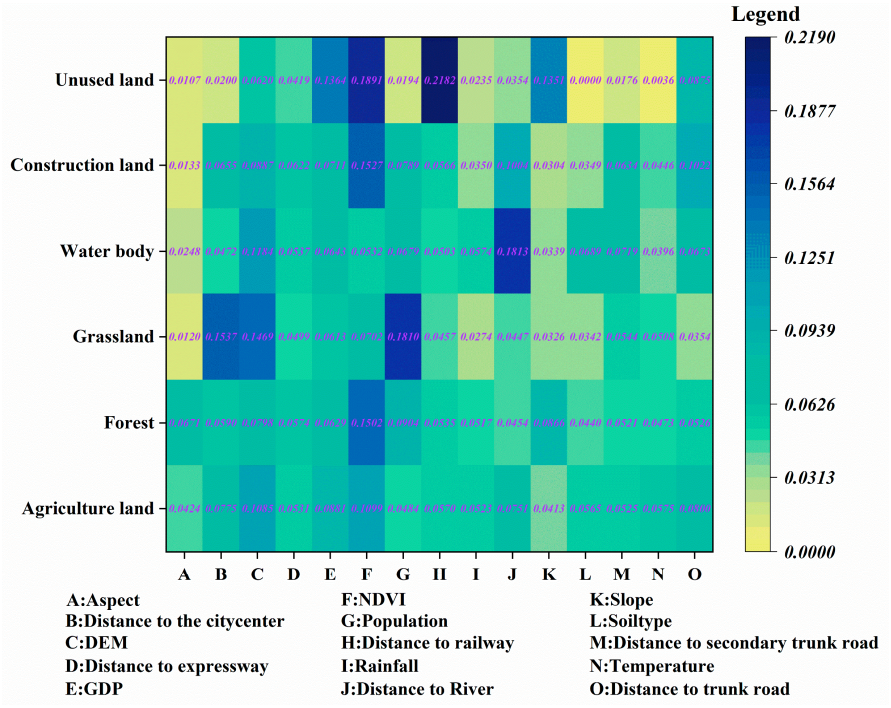

Figure 10. Contribution of the 15 drivers to the land use types.

Figure 11 shows the average contribution rate of each driver to the LUCC. Our findings indicated that a significant disparity occurred in the contribution levels of the seven natural environmental factors, whereas there was a relative balance of the impact of the eight socioeconomic factors. The strongest influences were exerted by NDVI, DEM, distance to trunk road, GDP, distance to a river, and population, and all were >7%. NDVI had the most significant effect on LUCC, with a contribution of 13.76%. The aspect of slope has the smallest effect on carbon storage, contributing only 4.09%. Future population growth, urban expansion, road development, and ecological land pattern changes will greatly affect the changes in agricultural, forest, and construction land areas, resulting in the evolution of the spatiotemporal patterns of carbon storage in the PRDUA.

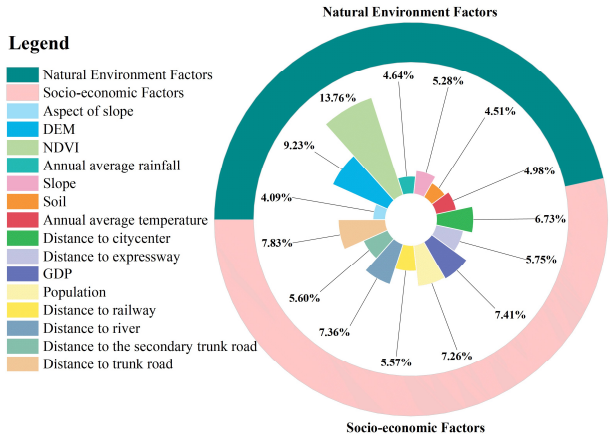

Figure 11. Average values of the 15 drivers for the main land types influencing LUCC.

3.4.2. Driving Mechanisms of the Change in Carbon Storage

In contrast, when the main drivers of carbon storage change are found indirectly by identifying the factors that influence the drivers of LUCC, the geoprobe approach can be used to further identify the factors that directly influence carbon storage. In this study, we identified 15 independent variables, comprising 7 natural environmental factors and 8 socioeconomic factors, as drivers in 2020. These variables were used as X, with carbon storage in the PRDUA for the same year serving as the dependent variable Y. Utilizing the geographical detector 'GD' R package, we quantified the explanatory power of each individual factor, represented by the q value, and determined the dominant interactive factors influencing changes in carbon storage (Table 9 and Figure 12).

Table 9. Explanatory power of every factor (q value).

Category	Driving Factors	q-Value
Natural Environment Factors	Soil	0.0954
	Slope	0.0340
	DEM	0.1385
	NDVI	0.0625
	Aspect of slope	0.0003
	Annual average rainfall	0.5383
	Annual average temperature	0.5559
Socioeconomic Factors	GDP	0.1661
	Population	0.0500
	Distance to river	0.0984
	Distance to railway	0.0184
	Distance to city center	0.0401
	Distance to trunk road	0.0509
	Distance to expressway	0.0133
	Distance to the secondary trunk road	0.0110

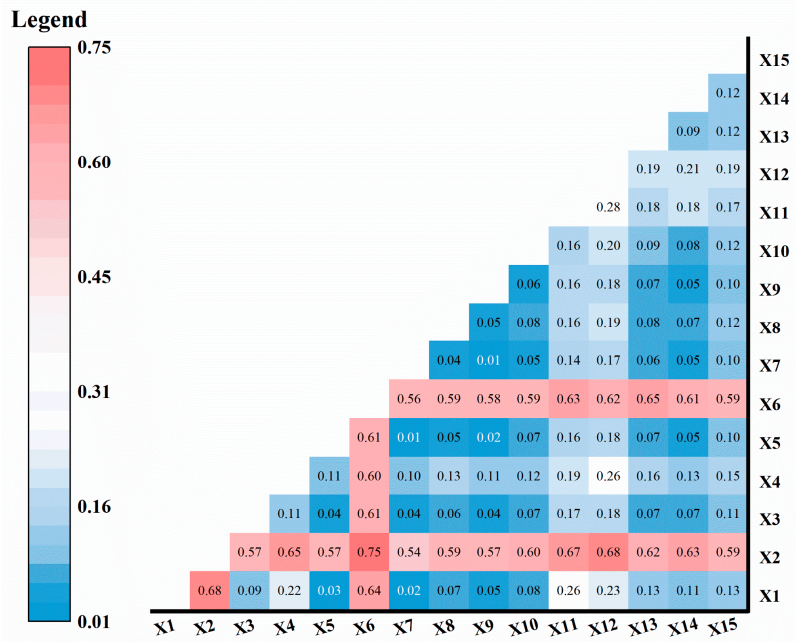

Figure 12. Dominant interactive factors of carbon storage changes in 2020 (X1 is distance to railway, X2 is annual average rainfall, X3 is slope, X4 is soi1, X5 is distance to the secondary trunk road, X6 is annual average temperature, X7 is aspect of slope, X8 is sistance to city center, X9 is distance to expressway, X10 is distance to trunk road, X11 is DEM, X12 is GDP, X13 is NDVI, X14 is population, X15 is distance to river).

The interactions between these drivers and changes in carbon storage predominantly manifested as nonlinear and double-factor enhancements. Specifically, carbon storage variations were significantly influenced by natural environmental factors, such as DEM, annual average rainfall, and annual average temperature. Socioeconomic factors were mainly influenced by GDP, distance from rivers, distance to the trunk road, and population size.

The results in Table 9 indicate that the single drivers with the greatest impact on carbon storage are the following, which all have q values greater than 0.05: annual average temperature (0.5559), annual average rainfall (0.5383) > GDP (0.1661) > DEM (0.1385), distance to river (0.0984) > soil (0.0954) > NDVI (0.0625) > distance to trunk road (0.0509), population (0.0500). The five groups with a higher explanatory power for carbon storage changes were as follows: X2∩X6 (0.75) > X1∩X2 (0.68) = X2∩X12 (0.68) > X2∩X11 (0.67) > X2∩X4 (0.65) = X6∩X13 (0.65) (Figure 12).

4. Discussion

This study coupled the PLUS and InVEST models to explore spatiotemporal changes in land use and carbon storage and their influencing factors in the PRDUA under multiple scenarios in 2030–2050. Although there are some uncertainties, these results are reliable and reasonable.

4.1. Response Relationship between Carbon Storage and Land Use Change

The LUCC is a significant driver of fluctuations in carbon storage in terrestrial ecosystems. Carbon storage plays a pivotal role in the maintenance of regional carbon cycles. The PRDUA exhibits distinctive patterns in carbon storage characterized by a configuration of "high around the periphery, low in the center" and "high in the north, low in the south". This is because of the more mature urbanization in the south-central part of the PRDUA, led by Shenzhen, Guangzhou, and Zhuhai, with urbanization levels of 99.83%, 86.18%, and 90.61%, respectively. The northern and western parts are dominated by Huizhou and Zhaoqing, which have large urban areas with urbanization levels of 72.61% and 50.97%, respectively. Furthermore, the forest coverage in the Huizhou and Zhaoqing areas is 63.98% and 72.7%, respectively [39]. The land use transfer matrix of the PRDUA from 2010 to 2020 revealed a decrease in the total carbon storage. In the three projected scenarios, carbon storage in the ND, CPD, and EPD scenarios in 2050 was 896.15 $\times$ 10^6 Mg, 889.44 $\times$ 10^6 Mg, and 923.45 $\times$ 10^6 Mg, respectively. Diversified land use changes have a significant impact on ecosystem carbon storage. For instance, the CPD scenario resulted in a pronounced decline in ecosystem carbon storage, whereas the EPD scenario ensured continuous development while increasing forest land and slowing the rate of decrease in agricultural land and grassland through sustained ecological protection measures such as afforestation, thereby achieving an increase in carbon storage.

4.2. Characterization of Carbon Storage Dynamics under Different Scenario Simulations

This study incorporated three socioeconomic development scenarios: ND, CPD, and EPD. The ND and CPD scenarios reflect the current urbanization trend driven by economic growth and development. However, this approach may not be sustainable in the long term. Therefore, this study also considers an EPD scenario that prioritizes environmental conservation, which is a more sustainable approach. EPD scenarios are characterized by a diverse range of features and pursue the principle of sustainable development, which is the primary objective of urban development in the current era.

Natural protection areas were defined as the limits of land use conversion to simulate carbon storage in the PRDUA for 2030, 2040, and 2050. The area available for restriction was limited, and the proportion of land suitable for reforestation was relatively low because of the maturity of urbanization in the study area. Consequently, the results of this study indicated that the total carbon storage in the three scenarios (ND, CPD, and EPD) was relatively similar. Even in the conservation development scenario, the increase in carbon storage was relatively modest. However, this does not imply that conservation development

has no merit. The total carbon storage in the ND and CPD scenarios is projected to decrease from 2030 to 2050.

4.3. Influence of Diverse Driving Factors on Carbon Storage

The results showed that the main factors affecting carbon storage were population, NDVI, DEM, distance to the railway, and GDP. These results are consistent with earlier studies [40–42]. Among the drivers that have a significant impact on carbon storage, the annual average temperature, annual average rainfall, soil, NDVI, and DEM are natural drivers, whereas GDP, population, and distance to the railway are socioeconomic drivers. Distance to railways is frequently overlooked and rarely incorporated into studies. The regional population and GDP levels had a significant influence on the expansion of construction land and the utilization of unused land. Although urban expansion may have direct economic benefits, it may also affect the ecology and reduce the carbon storage capacity of regional ecosystems. Furthermore, urban expansion is a significant contributor to increases in carbon emissions. Consequently, there is an urgent need to balance urban economic development with ecological preservation.

4.4. Research Limitation and Suggestions for Future Land Use Planning

This study integrates the PLUS and InVEST models to evaluate carbon storage in future ecosystems. The assessment results provide reliable and accurate forecasts of large-scale, long-term changes in ecosystem carbon reserves. However, it is important to note that the assessment is primarily based on land use changes. Additionally, a key limitation of the InVEST model is its assumption of constant carbon density over both space and time and its inability to account for potential dynamic variations. In reality, carbon density may fluctuate in response to natural environmental factors, which introduces uncertainty into the model's predictions. Moreover, given that ecological conservation is influenced by multiple policy interventions, a more comprehensive consideration of protective measures coupled with a quantitative analysis of the extent of these interventions would facilitate a deeper investigation of the impact of policy-driven conservation efforts on carbon storage in the ecological environment.

Government policies are mandatory and efficient for land use conversion, and the introduction of relevant policies has played a guiding role in land use changes [41]. The study area is predominantly forest and agricultural land, which are the land use types that mainly contribute to carbon storage. The expansion of urban areas was a significant factor in the reduction in forest and agricultural land in the PRDUA. To mitigate the adverse effects of urban expansion, it is essential to ensure that urban construction planning is accompanied by the active promotion of afforestation, the return of agricultural land to forests, and the delineation of ecological protection zones. Furthermore, it is necessary to control the rate of urban expansion, strengthen the protection of agricultural land, and ensure regional food security. Moreover, it is necessary to minimize the occupation of forest and water bodies and promote housing policies that will reduce population inflow to ecological zones caused by population growth and housing constraints [43].

5. Conclusions

Based on the PLUS and InVEST models, this study analyzed the spatiotemporal characteristics of land use and carbon storage in the PRDUA in 2010 and 2020 as the basic research periods. Moreover, it further simulated and predicted differences in land use and carbon storage changes in the PRDUA under three development scenarios (ND, CPD, and EPD) from 2030 to 2050. Status quo analyses, prediction simulations, and driving effect analyses were performed, with 2010 and 2020 acting as the basic research periods. This study further simulated and predicted the differences in changes in land use and carbon storage in the PRDUA under the three development scenarios from 2030 to 2050. Finally, this study employed both direct and indirect perspectives to comprehensively analyze the drivers of changes in carbon storage, thus providing theoretical support for the rational

formulation of land use policies and facilitating the acceleration of carbon neutrality efforts in the PRDUA. The main conclusions can be summarized as follows.

(1) From 2010 to 2020, agricultural and forest land in the PRDUA will decrease by 385.65 km^2 and 547.22 km^2, respectively, with the decrease accounting for 0.43% and 0.13% of their respective areas. Uncultivated land area will show the largest decrease (8.23%). Construction land area will increase sharply in both total area (952.64 km^2) and magnitude (1.33%). Changes in land use will decrease carbon storage in the study area by 9.52×10^6 Mg in 10 years at a rate of 1.02%. The spatial distribution of carbon storage will generally increase from the central to peripheral areas.

(2) LUCC in the PRDUA from 2020 to 2050 under the three scenarios showed obvious differences. Under the ND and CPD scenarios, agricultural land and forest land show the greatest decreases in area, while construction land showed the greatest increases. Under the EPD scenario, forest and construction land showed the greatest increases while agricultural land and grassland showed the greatest decreases. In the ND, CPD, and EPD scenarios, the land type with the largest area increase was construction land, with increases of 2011.16 km^2, 2816.20 km^2, and 100.04 km^2, respectively, while the land types with the largest decrease were agriculture land, agricultural land, and grassland, with decreases of 1075.39 km^2, 1445.63 km^2, and 124.62 km^2, respectively.

(3) Changes in carbon storage in the PRDUA under the ND, CPD, and EPD scenarios were -25.82×10^6 Mg, -32.54×10^6 Mg, and $+1.48 \times 10^6$ Mg, respectively, while the spatial distribution of carbon storage under the three scenarios showed similar clustering characteristics. High carbon storage values were mainly observed in the northeast, northwest, southwest, and city intersections, including Huizhou, Zhaoqing, and Jiangmen. Low carbon storage values were mainly located in the middle and southern areas, including Guangzhou, Shenzhen, Foshan, Dongguan, Zhuhai, and Zhongshan.

(4) Distance to railway, population, GDP, DEM, and NDVI were the main drivers of the spatial differentiation of LUCC in the PRDUA. The contributions of natural environmental factors (e.g., NDVI and DEM) to changes in agricultural land, forest, grassland, water bodies, construction land, and unused land were 46.84%, 52.67%, 37.41%, 39.62%, 39.96%, and 42.4%, respectively. The interactions between the 15 drivers and changes in carbon storage were predominantly manifested as nonlinear enhancement and double-factor enhancement.

Author Contributions: Conceptualization, J.C., H.C. (Hui Chi) and N.L.; Methodology, J.C., H.C. (Hui Chi) and N.L.; Software, J.C. and N.L.; Validation, J.C. and H.C. (Hui Chi); Formal analysis, J.C.; Investigation, J.C., N.L., H.C. (Hanqing Chen) and S.Y.; Resources, N.L., H.C. (Hanqing Chen) and S.Y.; Data curation, J.B.; Writing—original draft, J.C.; Writing—review & editing, H.C. (Hui Chi); Visualization, J.C. and J.Y.; Supervision, H.C. (Hui Chi); Project administration, H.C. (Hui Chi); Funding acquisition, N.L., J.B. and H.C. (Hanqing Chen). All authors have read and agreed to the published version of the manuscript.

Funding: This work was supported by the National Natural Science Foundation of China (NO. 42201029), the Guangdong Ocean University Research Start-up Fee Grant (NO. 060302072406), The 2023 Guangdong Undergraduate Colleges and Universities Teaching Quality and Teaching Reform Project Construction Project (NO. 010202072203).

Data Availability Statement: The data that support the findings of this study are available from the corresponding author upon reasonable request.

Conflicts of Interest: Author Suqin Yang was employed by Guangdong Yuehai Water Investment Co., Ltd. The remaining authors declare that the research was conducted in the absence of any commercial or financial relationships that could be construed as a potential conflict of interest.

References

1. Jeffry, L.; Ong, M.Y.; Nomanbhay, S.; Mofijur, M.; Mubashir, M.; Show, P.L. Greenhouse gases utilization: A review. *Fuel* **2021**, mboxemph301, 121017. [CrossRef]

2. Biermann, F.; Kanie, N.; Kim, R.E. Global governance by goal-setting: The novel approach of the UN Sustainable Development Goals. *Curr. Opin. Environ. Sustain.* **2017**, *26*, 26–31. [CrossRef]
3. Li, J.; Guo, X.; Chuai, X.; Xie, F.; Yang, F.; Gao, R.; Ji, X. Reexamine China's terrestrial ecosystem carbon balance under land use-type and climate change. *Land Use Policy* **2021**, *102*, 105275. [CrossRef]
4. Wang, Y.; Quan, S.; Tang, X.; Hosono, T.; Hao, Y.; Tian, J.; Pang, Z. Organic and inorganic carbon sinks reduce long-term deep carbon emissions in the continental collision margin of the southern Tibetan Plateau: Implications for Cenozoic climate cooling. *J. Geophys. Res. Solid Earth* **2024**, *129*, e2024JB028802. [CrossRef]
5. Qiu, S.; Yang, H.; Zhang, S.; Huang, S.; Zhao, S.; Xu, X.; He, P.; Zhou, W.; Zhao, Y.; Yan, N. Carbon storage in an arable soil combining field measurements, aggregate turnover modeling and climate scenarios. *Catena* **2023**, *220*, 106708. [CrossRef]
6. Bai, X.; Zhang, S.; Smith, P.; Li, C.; Xiong, L.; Du, C.; Xue, Y.; Li, Z.; Long, M.; Li, M. Resolving controversies surrounding carbon sinks from carbonate weathering. *Sci. China Earth Sci.* **2024**, *67*, 2705–2717. [CrossRef]
7. Sun, J.; Zhang, Y.; Qin, W.; Chai, G. Estimation and simulation of forest carbon stock in Northeast China forestry based on future climate change and LUCC. *Remote Sens.* **2022**, *14*, 3653. [CrossRef]
8. Luo, K.; Wang, H.; Ma, C.; Wu, C.; Zheng, X.; Xie, L. Carbon sinks and carbon emissions balance of land use transition in Xinjiang, China: Differences and compensation. *Sci. Rep.* **2022**, *12*, 22456. [CrossRef]
9. Wang, L.; Zhu, R.; Yin, Z.; Chen, Z.; Fang, C.; Lu, R.; Zhou, J.; Feng, Y. Impacts of land-use change on the spatio-temporal patterns of terrestrial ecosystem carbon storage in the Gansu Province, Northwest China. *Remote Sens.* **2022**, *14*, 3164. [CrossRef]
10. Olalekan, M.R.; Ilesanmi, A.; Alima, O.; Omini, D.E. Exploring How Human Activities Disturb the Balance of Biogeochemical Cycles: Evidence from the Carbon, Nitrogen and Hydrologic Cycles. *Res. World Agric. Econ.* **2021**, *2*, 23–44. [CrossRef]
11. Olorunfemi, I.E.; Olufayo, A.A.; Fasinmirin, J.T.; Komolafe, A.A. Dynamics of land use land cover and its impact on carbon stocks in Sub-Saharan Africa: An overview. *Environ. Dev. Sustain.* **2022**, *24*, 40–76. [CrossRef]
12. Sharma, S.; MacKenzie, R.A.; Tieng, T.; Soben, K.; Tulyasuwan, N.; Resanond, A.; Blate, G.; Litton, C.M. The impacts of degradation, deforestation and restoration on mangrove ecosystem carbon stocks across Cambodia. *Sci. Total Environ.* **2020**, *706*, 135416. [CrossRef]
13. Aitkenhead, M.; Coull, M. Mapping soil profile depth, bulk density and carbon stock in Scotland using remote sensing and spatial covariates. *Eur. J. Soil Sci.* **2020**, *71*, 553–567. [CrossRef]
14. Sun, W.; Liu, X. Review on carbon storage estimation of forest ecosystem and applications in China. *For. Ecosyst.* **2020**, *7*, 1–14. [CrossRef]
15. Piao, S.; He, Y.; Wang, X.; Chen, F. Estimation of China's terrestrial ecosystem carbon sink: Methods, progress and prospects. *Sci. China Earth Sci.* **2022**, *65*, 641–651. [CrossRef]
16. Tian, L.; Wu, X.; Tao, Y.; Li, M.; Qian, C.; Liao, L.; Fu, W. Review of remote sensing-based methods for forest aboveground biomass estimation: Progress, challenges, and prospects. *Forests* **2023**, *14*, 1086. [CrossRef]
17. Wang, R.-Y.; Mo, X.; Ji, H.; Zhu, Z.; Wang, Y.-S.; Bao, Z.; Li, T. Comparison of the CASA and InVEST models' effects for estimating spatiotemporal differences in carbon storage of green spaces in megacities. *Sci. Rep.* **2024**, *14*, 5456. [CrossRef] [PubMed]
18. Hu, Y.; Li, Y.; Zhang, H.; Liu, X.; Zheng, Y.; Gong, H. The trajectory of carbon emissions and terrestrial carbon sinks at the provincial level in China. *Sci. Rep.* **2024**, *14*, 5828. [CrossRef]
19. Kafy, A.-A.; Saha, M.; Fattah, M.A.; Rahman, M.T.; Duti, B.M.; Rahaman, Z.A.; Bakshi, A.; Kalaivani, S.; Rahaman, S.N.; Sattar, G.S. Integrating forest cover change and carbon storage dynamics: Leveraging Google Earth Engine and InVEST model to inform conservation in hilly regions. *Ecol. Indic.* **2023**, *152*, 110374. [CrossRef]
20. Tian, L.; Tao, Y.; Fu, W.; Li, T.; Ren, F.; Li, M. Dynamic simulation of land use/cover change and assessment of forest ecosystem carbon storage under climate change scenarios in Guangdong Province, China. *Remote Sens.* **2022**, *14*, 2330. [CrossRef]
21. Wang, Z.; Zeng, J.; Chen, W. Impact of urban expansion on carbon storage under multi-scenario simulations in Wuhan, China. *Environ. Sci. Pollut. Res.* **2022**, *29*, 45507–45526. [CrossRef] [PubMed]
22. Deng, Y.; Yao, S.; Hou, M.; Zhang, T.; Lu, Y.; Gong, Z.; Wang, Y. Assessing the effects of the Green for Grain Program on ecosystem carbon storage service by linking the InVEST and FLUS models: A case study of Zichang county in hilly and gully region of Loess Plateau. *J. Nat. Resour.* **2020**, *35*, 826–844. [CrossRef]
23. Tang, L.; Ke, X.; Zhou, Q.; Wang, L.; Koomen, E. Projecting future impacts of cropland reclamation policies on carbon storage. *Ecol. Indic.* **2020**, *119*, 106835. [CrossRef]
24. Shaffer, J.A.; Roth, C.L.; Mushet, D.M. Modeling effects of crop production, energy development and conservation-grassland loss on avian habitat. *PLoS ONE* **2019**, *14*, e0198382. [CrossRef]
25. Li, M.; Liang, D.; Xia, J.; Song, J.; Cheng, D.; Wu, J.; Cao, Y.; Sun, H.; Li, Q. Evaluation of water conservation function of Danjiang River Basin in Qinling Mountains, China based on InVEST model. *J. Environ. Manag.* **2021**, *286*, 112212. [CrossRef]
26. Hu, W.; Li, G.; Gao, Z.; Jia, G.; Wang, Z.; Li, Y. Assessment of the impact of the Poplar Ecological Retreat Project on water conservation in the Dongting Lake wetland region using the InVEST model. *Sci. Total Environ.* **2020**, *733*, 139423. [CrossRef] [PubMed]
27. Zhang, Z.; Hu, B.; Jiang, W.; Qiu, H. Identification and scenario prediction of degree of wetland damage in Guangxi based on the CA-Markov model. *Ecol. Indic.* **2021**, *127*, 107764. [CrossRef]
28. Liang, X.; Liu, X.; Li, X.; Chen, Y.; Tian, H.; Yao, Y. Delineating multi-scenario urban growth boundaries with a CA-based FLUS model and morphological method. *Landsc. Urban Plan.* **2018**, *177*, 47–63. [CrossRef]

29. Huang, D.; Huang, J.; Liu, T. Delimiting urban growth boundaries using the CLUE-S model with village administrative boundaries. *Land Use Policy* **2019**, *82*, 422–435. [CrossRef]
30. Liang, X.; Guan, Q.; Clarke, K.C.; Liu, S.; Wang, B.; Yao, Y. Understanding the drivers of sustainable land expansion using a patch-generating land use simulation (PLUS) model: A case study in Wuhan, China. *Comput. Environ. Urban Syst.* **2021**, *85*, 101569. [CrossRef]
31. Guo, W.; Teng, Y.; Li, J.; Yan, Y.; Zhao, C.; Li, Y.; Li, X. A new assessment framework to forecast land use and carbon storage under different SSP-RCP scenarios in China. *Sci. Total Environ.* **2024**, *912*, 169088. [CrossRef] [PubMed]
32. Wei, Q.; Abudureheman, M.; Halike, A.; Yao, K.; Yao, L.; Tang, H.; Tuheti, B. Temporal and spatial variation analysis of habitat quality on the PLUS-InVEST model for Ebinur Lake Basin, China. *Ecol. Indic.* **2022**, *145*, 109632. [CrossRef]
33. Wu, X.; Huang, Y.; Gao, J. Impact of industrial agglomeration on new-type urbanization: Evidence from Pearl River Delta urban agglomeration of China. *Int. Rev. Econ. Financ.* **2022**, *77*, 312–325. [CrossRef]
34. Du, S.; Zhou, Z.; Huang, D.; Zhang, F.; Deng, F.; Yang, Y. The Response of Carbon Stocks to Land Use/Cover Change and a Vulnerability Multi-Scenario Analysis of the Karst Region in Southern China Based on PLUS-InVEST. *Forests* **2023**, *14*, 2307. [CrossRef]
35. Li, M.; Gao, Q.; Yu, T. Using appropriate Kappa statistic in evaluating inter-rater reliability. Short communication on "Groundwater vulnerability and contamination risk mapping of semi-arid Totko river basin, India using GIS-based DRASTIC model and AHP techniques". *Chemosphere* **2023**, *328*, 138565. [CrossRef] [PubMed]
36. Zhang, T.; Song, B.; Han, G.; Zhao, H.; Hu, Q.; Zhao, Y.; Liu, H. Effects of coastal wetland reclamation on soil organic carbon, total nitrogen, and total phosphorus in China: A meta-analysis. *Land Degrad. Dev.* **2023**, *34*, 3340–3349. [CrossRef]
37. Wang, R.-Y.; Cai, H.; Chen, L.; Li, T. Spatiotemporal Evolution and Multi-Scenario Prediction of Carbon Storage in the GBA Based on PLUS–InVEST Models. *Sustainability* **2023**, *15*, 8421. [CrossRef]
38. Zhang, Y.; Naerkezi, N.; Zhang, Y.; Wang, B. Multi-Scenario Land Use/Cover Change and Its Impact on Carbon Storage Based on the Coupled GMOP-PLUS-InVEST Model in the Hexi Corridor, China. *Sustainability* **2024**, *16*, 1402. [CrossRef]
39. Yang, C.; Liu, H.; Li, Q.; Cui, A.; Xia, R.; Shi, T.; Zhang, J.; Gao, W.; Zhou, X.; Wu, G. Rapid urbanization induced extensive forest loss to urban land in the Guangdong-Hong Kong-Macao Greater Bay Area, China. *Chin. Geogr. Sci.* **2021**, *31*, 93–108. [CrossRef]
40. Wang, R.; Zhao, J.; Chen, G.; Lin, Y.; Yang, A.; Cheng, J. Coupling PLUS–InVEST model for ecosystem service research in Yunnan Province, China. *Sustainability* **2022**, *15*, 271. [CrossRef]
41. Liu, K.; Zhang, C.; Zhang, H.; Xu, H.; Xia, W. Spatiotemporal Variation and Dynamic Simulation of Ecosystem Carbon Storage in the Loess Plateau Based on PLUS and InVEST Models. *Land* **2023**, *12*, 1065. [CrossRef]
42. Li, P.; Chen, J.; Li, Y.; Wu, W. Using the InVEST-PLUS model to predict and analyze the pattern of ecosystem carbon storage in Liaoning Province, China. *Remote Sens.* **2023**, *15*, 4050. [CrossRef]
43. Xu, A.; Song, M.; Wu, Y.; Luo, Y.; Zhu, Y.; Qiu, K. Effects of new urbanization on China's carbon emissions: A quasi-natural experiment based on the improved PSM-DID model. *Technol. Forecast. Soc. Chang.* **2024**, *200*, 123164. [CrossRef]